

Numerical Investigation on non-premixed Rotating Detonation Engine with Different Exhaust Nozzle Configurations

Sainan Xue, Hu Ma, Gaoyang Ge, Zhenjuan Xia, Can Xu, ChangFei Zhuo
*School of Mechanical and Engineering, Nanjing University of Science & Technology
Nanjing, China;*

Abstract

Three-dimensional numerical simulations were conducted on a non-premixed rotating detonation engine (RDE) with different exhaust nozzles (i.e. without a nozzle, with a divergent nozzle, with a convergent nozzle, and with a Laval nozzle). Aside from describing the flow-field structure inside the chamber, the detonation wave height, the average propagation velocity of the detonation wave, and the outlet Mach number were also investigated. It is found that the minimum cross section reaches a critical state for the convergent nozzle and the Laval nozzle, but there is a subsonic region at outlet for the divergent nozzle. By the reflected shock waves, the convergent and Laval nozzles make the flow-fields more complex in chamber, but it makes the Mach number distribution more homogeneous in exit.

Keywords: Rotating detonation engine; Three-dimensional numerical simulation; nozzle; Non-premixed; Propulsive performance.

1. Introduction

Detonation combustion is approximately constant volume combustion. Detonation wave can make the temperature and pressure of reactants rise rapidly. Compared with constant pressure combustion, detonation combustion has some obvious advantages, such as rapid heat release, high thermodynamic efficiency, pressure-gain and so on. Rotating detonation engine (RDE) with detonation combustion, in which annular combustion chamber is usually adopted, has drawn considerable attention over the past few decades[1-2].

Furthermore, Poland, France, Japan and China have also carried out many investigations in RDE[3-6]. It is worth noting that some achievements have also been made in studying nozzles, which can prompt detonation products to expand more fully. Yi et al. [7] studied the effects of different nozzle configurations on RDE propulsive performance by three-dimensional numerical simulations. Matthew et al. [8] conducted experimental studies on RDE with four different nozzles to study the effects of equivalence ratio and mass flow rate. James et al. [9] used OpenFOAM to numerically calculate the premixed RDE with five different nozzle configurations, and analyzed the variation of some parameters, such as total pressure, Mach number, and total temperature. Yetao S. [10] conducted three-dimensional numerical calculations with one-step chemical reaction model to investigate the propulsive performance of four different nozzles, proved that nozzle can greatly improve the engine's performance.

Nevertheless, studies on the influence of different exhaust nozzle configurations on RDE are still limited. Non-premixed injection methods of fuel and oxidant were used to obtain rotating detonation wave in experiments of RDE. Therefore, this work would adopt three-dimensional numerical simulation method to investigate non-premixed H₂/Air RDE with four different configurations (i.e. without a nozzle, with a divergent nozzle, with a convergent nozzle and with a Laval nozzle). This paper not only shows and analyzes the flow-field structure inside the chamber, but also studies the performance of RDE.

2. Numerical Method and Model

2.1 Calculation method and validation

The Three-dimensional reactive Euler equations, which were used in this paper to simulate strong convective chemical non-equilibrium flow. Transport properties, such as flow viscosity, heat conduction and diffusion, were ignored in these equations.

The three-dimensional reactive Euler equations are discretized based on the finite volume method. Primitive variables are reconstructed by a third-order accurate MUSCL scheme to improve the accuracy of spatial discretization. Convection flux quantities are discretized by the AUSMPW+ scheme. A second-order Runge–Kutta time marching is adopted for unsteady problems. In this work, as combustion chemical kinetic model, a 7 components and 8-step chemical reaction model proposed by Spiegler is used for H₂/Air mixture. [11] The reactions are shown in table 1. The chemical reaction rate is calculated by the Arrhenius equation. The time-operator splitting algorithm is used to address the stiff problem of chemical reaction.

Table 1: 7 components and 8-step chemical reaction for H₂/Air(O₂+3.76N₂) mixture

| Number | Reaction | A | b | $E_0/R_0/K$ |
|--------|--------------------------------------|--------|------|-------------|
| 1 | H ₂ +M=H+H+M | 5.5E18 | -1.0 | 51987.0 |
| 2 | O ₂ +M=O+O+M | 7.2E18 | -1.0 | 59340.0 |
| 3 | H ₂ O+M=H+OH+M | 5.2E21 | -1.5 | 59386.0 |
| 4 | OH+M=O+H+M | 8.5E18 | -1.0 | 50830.0 |
| 5 | H ₂ O+O=OH+OH | 5.8E13 | 0.0 | 9095.0 |
| 6 | H ₂ O+H=OH+H ₂ | 8.4E13 | 0.0 | 10116.0 |
| 7 | H+O ₂ =OH+O | 2.2E14 | 0.0 | 8455.0 |
| 8 | H ₂ +O=OH+H | 7.5E13 | 0.0 | 5586.0 |

To validate this numerical method for the calculation, C-J parameters of the detonation wave, such as pressure, temperature and propagation velocity, were simulated by the method. Relative to the theoretical value calculated by CEA (Chemical Equilibrium with Applications) software, the errors of C-J parameters calculated by the numerical method are 0.99%, 1.97% and 0.31%, respectively.

2.2 Physical model

H₂ is injected from a plenum to the detonation chamber through 90 micro holes, which are uniformly distributed along the circumferential direction, as shown in Fig. 1. Air is injected axially from a plenum through a convergent-divergent circular slot. Figure 2 is the cross-sectional view of combustion chamber with different exhaust nozzles. The inner radius R_i and outer radius R_o of annular chamber are 35 mm and 40 mm, respectively. The channel width of chamber is 5 mm. The axial length L of constant chamber is 40 mm. The corresponding sizes of each model are given in Fig. 2. For the Laval nozzle, width of the nozzle throat is 2.5 mm. The commercial software ICEM is employed for meshing, and hexahedral structure grid is adopted. In this simulation, the maximum grid resolution is 0.35 mm, and more refined grids are applied at the place with sharp change of flow. The grid resolution can meet the requirements of the numerical simulation.

Three-dimensional computation domain of the engine without a nozzle, corresponding to model 1, is shown in Fig. 1. The mass flow rate of H₂ inlet and air inlet are shown in table 2 for different models. Total temperature of H₂ inlet and air inlet are 290 K for all cases. The back pressure at engine exit, p_b , is 1 atm. The average equivalence ratio of H₂/air mixture is 1.5. Furthermore, the adiabatic, sliding, and non-catalytic walls are applied.

Table 2: Calculation parameters

| cases | $\dot{m}_{air}/(g/s)$ | $\dot{m}_{H_2}/(g/s)$ | T_{0air}/K | T_{0H_2}/K | p_b/atm |
|--------|-----------------------|-----------------------|--------------|--------------|-----------|
| case#1 | 120.50 | 5.50 | 290 | 290 | 1 |
| case#2 | 200.10 | 9.04 | 290 | 290 | 1 |
| case#3 | 241.12 | 11.04 | 290 | 290 | 1 |
| case#4 | 301.40 | 13.75 | 290 | 290 | 1 |
| case#5 | 361.68 | 16.57 | 290 | 290 | 1 |
| case#6 | 421.96 | 19.33 | 290 | 290 | 1 |

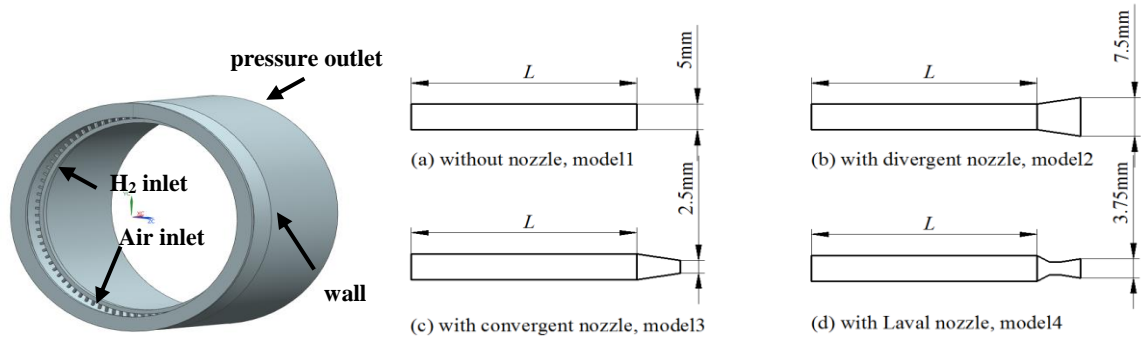


Figure 1: Computational domain of the RDE Figure2: Cross-section of combustion chamber and nozzles

3. Results and analysis

Figure 4 is the temperature contours of internal flow-fields for case#2 with different nozzles. According to the characteristics of temperature distribution, it can be clearly seen that the locations of the detonation wave front, oblique shock wave, fresh reactants and contact discontinuity (between fresh reactants and products), as indicated by black arrows in Fig.4. The white arrows indicates the propagation direction of the rotating detonation wave. Besides that, slip line and reflected shock waves can be observed in Fig. 4 (c) and Fig. 4 (d). The slip lines forms between two adjacent recirculating detonation products. The reflected shock waves are caused by the convergent segment of exhaust nozzles.

The notable three-point intersection structure, as shown in the marked circle, is formed by the detonation wave front, the oblique shock wave and the contact discontinuity. The axial length from hydrogen injection holes to the three-point structure is defined as the height of rotating detonation wave. It can be seen from Fig.4 that the height for with divergent nozzle is the largest, and is close to that of without a nozzle. In addition, it will be obviously reduced when the convergent nozzle and the Laval nozzle are attached.

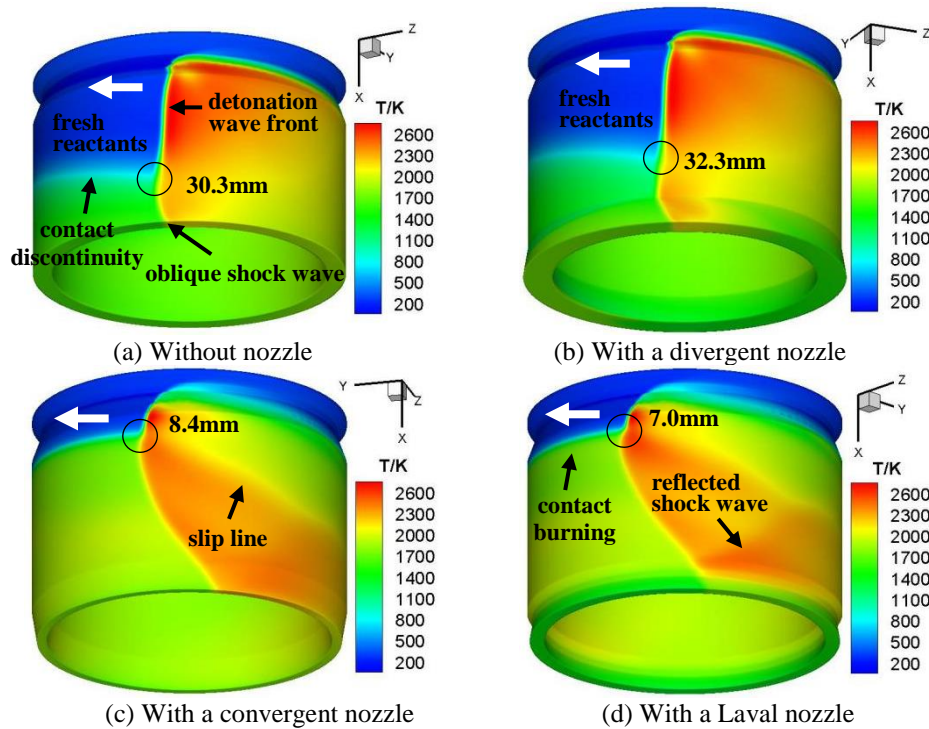


Figure 4: Temperature contours in RDE of case#2

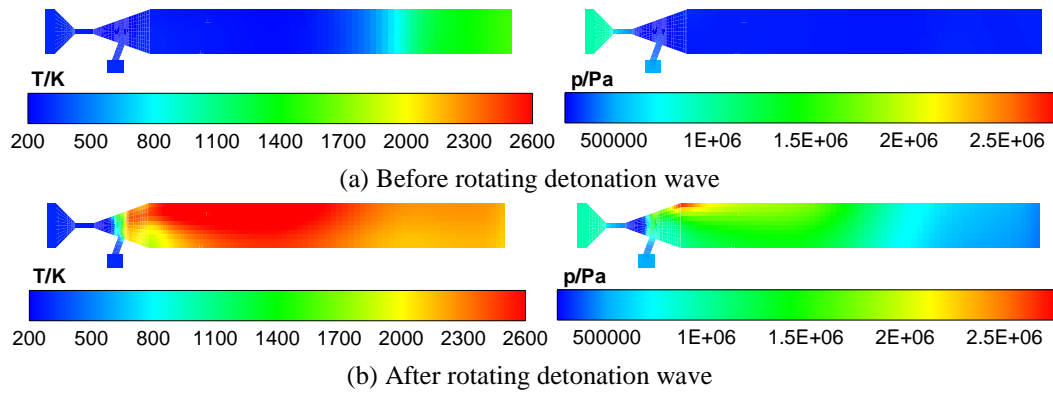
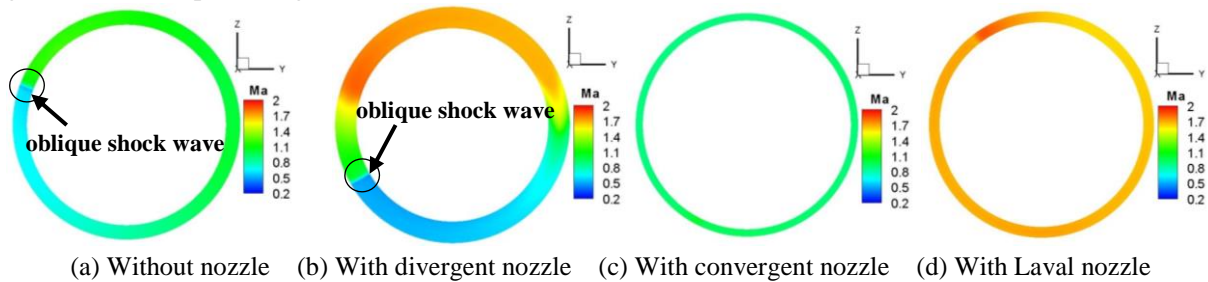


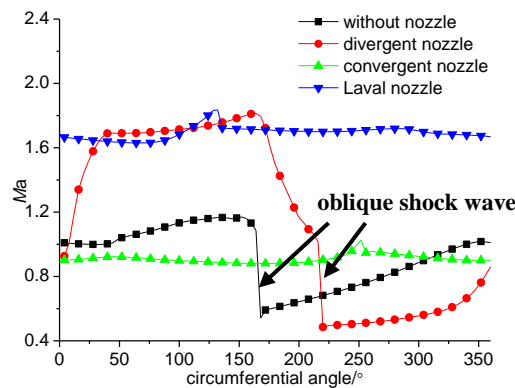
Figure 5: Temperature and pressure contours in case#2

The reason for this phenomenon is that the exit area of divergent nozzle is the largest, as shown in Fig.2, resulting in the decrease of average pressure in the detonation chamber, which is conducive to the filling of fresh reactants. However, with the addition of convergent nozzle and Laval nozzle, the exit areas will be obviously reduced, and the average pressure in chambers will rise drastically, which is detrimental to the filling of fresh reactants and therefore leads to a corresponding decrease in the height of rotating detonation wave.

Figure 5 is the temperature and pressure slice contours before and after rotating detonation wave. Comparing Fig. 5 (a) with Fig. 5 (b), it can be found that the temperature and pressure after rotating detonation wave are significantly higher than that before rotating detonation wave. As can be seen from Fig. 5 (b), temperature near the chamber inlet is much higher than that of the exit, indicating that the detonation wave front is located at the head of detonation chamber. In addition, the temperature and pressure near the outer wall are higher than that of the inner wall. This is the result of curvature effect, bringing the pressure gradient and temperature gradient between the inner and outer walls.



(a) Without nozzle (b) With divergent nozzle (c) With convergent nozzle (d) With Laval nozzle



(e) Mach number distribution along circumferential direction ($\dot{m}_{Air}=200.10g/s$)

Figure 6: Mach number at the outlet of RDE for case#2

Figure 6 (a) ~ Figure 6 (d) are the contours of Mach number at the exit of chamber for case#2. As can be seen from Fig. 6(a), Mach number of the exit without a nozzle is divided into two parts, and there is an obvious dividing line between the two parts, as shown in the marked circle, which also suggests the location of oblique shock wave. The velocity before and after the oblique shock wave are subsonic and

supersonic, respectively. A mixed subsonic and supersonic flow can also be observed in Fig.6 (b). In contrast, Mach number distribution at exit is relatively more uniform for convergent nozzle, as shown in Fig. 6(c). Due to that the convergent geometry cannot make flow accelerate to supersonic, the Mach number is close to 1. Figure 6 (d) provides the Mach number at exit of Laval nozzle, it can be seen that the Mach number with Laval nozzle is the largest compared with other nozzles. This is due to that the convergent-divergent geometry of Laval nozzle can make subsonic flow continually accelerate to supersonic.

Figure 6 (e) shows the curves of Mach number distribution along the circumferential direction for different configurations. It can be seen that, for model 1 without nozzle, the exit Mach number is divided into two parts with a strong discontinuity, which corresponds to the oblique shock wave. Thus a part of the outflow is supersonic, and the rest is subsonic. In addition, the strong discontinuity is also observed in the divergent nozzle. However, Due to the Mach number of supersonic flow and subsonic flow will increased and decreased for divergent nozzle, respectively, the strong discontinuity is enlarged. Moreover, the discontinuities obviously weaken for convergent nozzle and Laval nozzle, and the Mach number of exit is less than 1 for convergent nozzle, while Mach number of exit is about 1.7 for Laval nozzle.

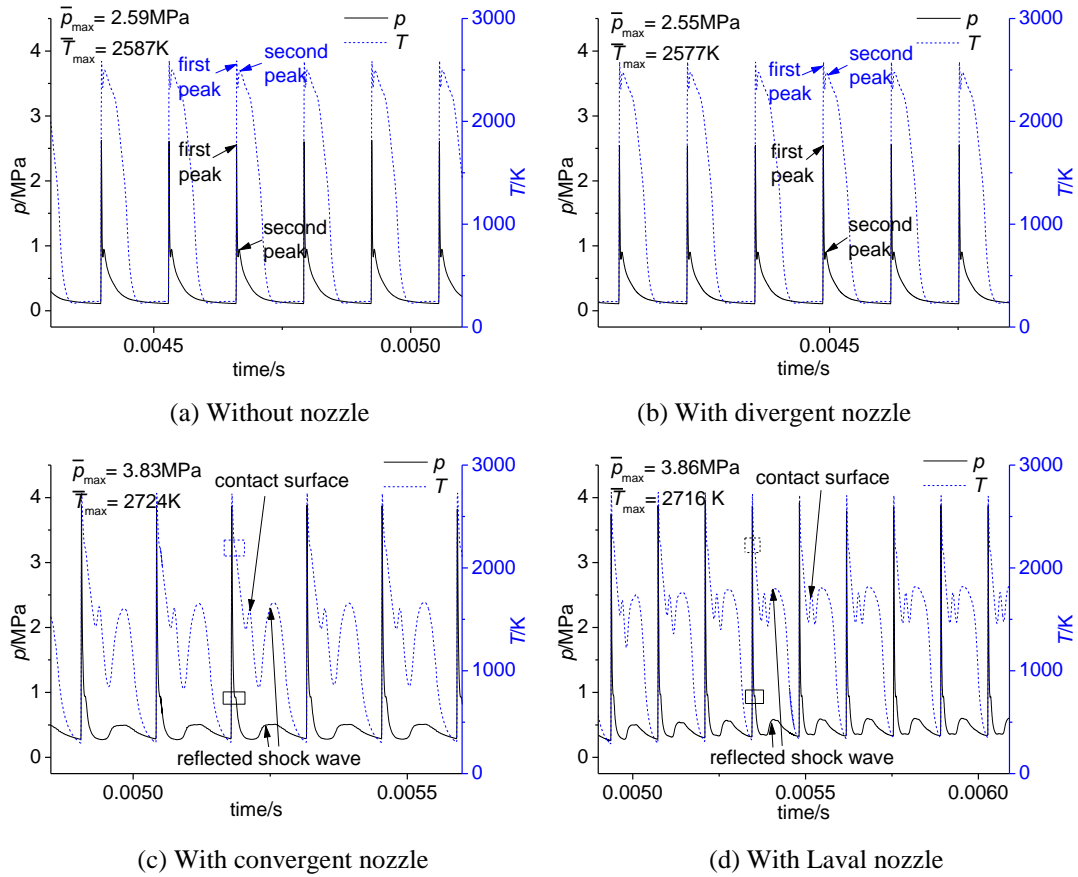


Figure 7: Pressure-time and temperature-time curves obtained at outside wall of combustion chamber in case#2

Figure 7 shows the variation of pressure and temperature with time at a fixed monitoring point for the four different configurations in case#2. The monitoring point is arranged on the outer wall of detonation chamber, and it is within the detonation wave height. From figure 7, it can be seen that pressure and temperature rise at the same time in each circulation, indicating the coupling of leading shock wave and the subsequent chemical reaction zone. The average pressure peak \bar{p}_{\max} and average temperature peak \bar{T}_{\max} of each model are recorded in the figures. It turns out that the \bar{p}_{\max} and \bar{T}_{\max} of convergent nozzle and Laval nozzle are obviously larger than the other two models. This is the result of the reduction of exit area that can lead to increasing average pressure in detonation chamber. In addition, as indicated in Fig. 7(a) and Fig.7 (b), both of the pressure-time curve and temperature-time curve show two peaks in one circulation.

The first peak corresponds to the detonation wave front, and the second peak corresponds to the compression wave, which is reflected from the divergent segment of injection structure. However, In Fig.7 (c) and Fig.7 (d), there are two intense fluctuations in the descending process of temperature. The first fluctuation, marked as “contact surface”, corresponds to the contact burning between detonation products and fresh reactants, and the burning is obvious when the chamber pressure increased due to the decrease of exit area. The second fluctuation, as indicated by “reflected shock wave”, is the reflection of oblique shock wave at the convergent segment of exhaust nozzle, and the corresponding pressure also fluctuates significantly. The contact burning and reflected shock wave can be clearly observed in Fig. 4 (c) and Fig. 4 (d).

4. Conclusions

For non-premixed rotating detonation engine, four nozzles with different air mass flow rate are investigated by three-dimensional numerical simulation. Based on the analysis of these calculation results, some conclusions are obtained as follows:

(1) The flow-fields of non-premixed rotating detonation wave for different nozzles are obtained. The reflected shock waves are all observed in convergent nozzle and Laval nozzle. The both nozzles make the flow-fields more complex in chamber by the reflected shock waves, but it makes the Mach number distribution more homogeneous in exit, compared with divergent nozzle or without nozzle.

(2) For without nozzle, the Mach number in exit includes supersonic, sonic and subsonic flow for smaller air mass flow rate, but it only has supersonic and sonic flow for higher air mass flow rate.

References

- [1] Lu, F.K., Braun, E.M., Rotating Detonation Wave Propulsion: Experimental Challenges, Modeling, and Engine Concepts (Invited), *Journal Of Propulsion And Power* Vol. 30, No. 5, 2014, pp.1125-1142.
- [2] Wolanski, P., Detonative Propulsion, *Proceedings of the Combustion Institute*, Vol. 34, pp. 125-158, 2013.
- [3] Nobuyuki T., Yusuke W., Takayuki K., and A.Koichi H. “Numerical estimation of the thrust performance on a rotating detonation engine for a hydrogen-oxygen mixture”, *Proceedings of the Combustion Institute*. 2015; 35:2005-2013.
- [4] YeTao S., Meng L., and JianPing W. “Numerical Investigation of Rotating Detonation Engine”, Propulsive Performance”, *Combustion Science and Technology*. 2010; 182:1586-1597.
- [5] Chao W., WeiDong L., ShiJie L., Luxin J., and Zhiyong L. “Experimental Verification of Air-breathing Continuous Rotating Detonation Fueled by Hydrogen”, *International Journal of Hydrogen Energy*. 2015; 1-9.
- [6] ChengLong Y., XiaoSong W., Hu M., Lei P, and Jian G. “Experimental Research on Initiation Characteristics of a Rotating Detonation Engine”, *Experimental Thermal and Fluid Science*. 2016; 71:154-163.
- [7] Yi T.H., Lou J., Turangan C., Khoo C.B., and Wolanski P. “Effect of Nozzle Shapes on the Performance of Continuously Rotating Detonation Engine”, *AIAA*. 2010-152.
- [8] Matthew L.F., Fred S., Tom K., and John H.. “Experimental Study of the Performance of a Rotating Detonation Engine with Nozzle”. *Journal of Propulsion and Power*. 2016; 32:674-681.
- [9] James B., Bayindir H.S., and Guillermo P. “Unsteady Performance of Rotating Detonation Engines with Different Exhaust Nozzles”, *Journal of Propulsion and Power*. 2017; 33:121-130.
- [10] YeTao S., Meng L., and JianPing W. “Continuous Detonation Engine and Effects of Different Types of Nozzle on Its Propulsion Performance”, *Chinese Journal of Aeronautics*. 2010; 23: 647-652.
- [11] Spiegler E., Wolfshtein M., Manheimer-Timmat Y. “A model of unmixedness for turbulent reacting flows”, *Acta Astronaut*. 1976; 3: 265 – 280.